RSC Advances

PAPER

View Article Online
View Journal | View Issue

Cite this: *RSC Adv.*, 2021, **11**, 13269

Efficient charge separation and transfer of a TaON/$BiVO_4$ heterojunction for photoelectrochemical water splitting†

Na Li,[ab] Yi Jiang,[*a] Xiaodi Wang,[a] Chongyang Hu,[a] Wenchao Jiang,[a] Siyuan Li[a] and Lixin Xia[*ab]

Received 5th February 2021
Accepted 14th March 2021

DOI: 10.1039/d1ra00974e

rsc.li/rsc-advances

The separation and transfer of photogenerated electron–hole pairs in semiconductors is the key point for photoelectrochemical (PEC) water splitting. Here, an ideal TaON/$BiVO_4$ heterojunction electrode was fabricated *via* a simple hydrothermal method. As $BiVO_4$ and TaON were in well contact with each other, high performance TaON/$BiVO_4$ heterojunction photoanodes were constructed. The photocurrent of the 2-TaON/$BiVO_4$ electrode reached 2.6 mA cm^{-2} at 1.23 V *vs.* RHE, which is 1.75 times as that of the bare $BiVO_4$. TaON improves the PEC performance by simultaneously promoting the photo-generated charge separation and surface reaction transfer. When a Co-Pi co-catalyst was integrated onto the surface of the 2-TaON/$BiVO_4$ electrode, the surface water oxidation kinetics further improved, and a highly efficient photocurrent density of 3.6 mA cm^{-2} was achieved at 1.23 V *vs.* RHE. The largest half-cell solar energy conversion efficiency for Co-Pi/TaON/$BiVO_4$ was 1.19% at 0.69 V *vs.* RHE, corresponding to 6 times that of bare $BiVO_4$ (0.19% at 0.95 V *vs.* RHE). This study provides an available strategy to develop photoelectrochemical water splitting of $BiVO_4$-based photoanodes.

Introduction

At present, the shortage of fossil fuels and increase of global warming have become very serious social and environmental problems. As a green energy source, solar energy is widely distributed. Hydrogen is also a type of clean energy with a high heating value. Therefore, the use of solar energy to produce hydrogen has attracted widespread attention.[1] Building a photoelectrochemical (PEC) cell to mimic the photosynthesis system is an effective method to realize the conversion of solar energy into hydrogen energy.[2–6] However, in a PEC system, the water oxidation reaction half reaction occurring in the photoanode involves light capture, charge separation, and complex surface reaction with multiple electron and proton transfer. Therefore, designing an efficient photoanode to accelerate the water oxidation process becomes the key to the development of PEC cells.

In recent years, semiconductors based on metal oxides, such as $BiVO_4$, TiO_2, and WO_3, have been widely used as photoanode materials.[7–11] $BiVO_4$, an n-type semiconductor with a band gap of 2.4 eV, is considered as one of the most promising alternative materials.[12] Under the irradiation of a sunlight AM 1.5 G, the solar-to-hydrogen efficiency (STH) can reach 9.2%,[13] which is close to the solar-powered water decomposition technology target (STH efficiency 10%).[14] However, the severe recombination of the electron–hole pair of $BiVO_4$ limits its development. Different strategies were adopted to enhance the PEC performance of $BiVO_4$,[15,16] such as elemental doping, nanostructure modification, loading cocatalysts and heterojunction construction. Among them, the construction of semiconductor heterojunctions with different materials is an effective approach to improve the PEC performance by enhancing the separation efficiency of photo-generated charges. Although there were numerous reports on heterojunction systems for $BiVO_4$-based semiconductors, such as $CaFe_2O_4$/$BiVO_4$,[17] V_2O_5/$BiVO_4$,[18] WO_3/$BiVO_4$ [19–21] and TiO_2/$BiVO_4$,[22,23] the construction of a high-efficiency heterojunction photoanode still faces great challenges.

Here, TaON/$BiVO_4$ heterojunction photoanodes were constructed, which exhibited a greatly improved PEC water oxidation activity compared to the bare $BiVO_4$ photoanode. The photocurrent of the 2-TaON/$BiVO_4$ photoanode reached 2.6 mA cm^{-2} at 1.23 V *vs.* RHE, which was 1.75-times that of $BiVO_4$. In order to enhance the surface water oxidation kinetics of the photoanode, the Co-Pi water oxidation catalyst was immobilized on the photoanode, and the PEC performance was further promoted. A high photocurrent density of 3.6 mA cm^{-2} was obtained for Co-Pi/TaON/$BiVO_4$ at 1.23 V *vs.* RHE.

[a]*College of Chemistry, Liaoning University, Shenyang 110036, Liaoning, China. E-mail: jiangyi@lnu.edu.cn; lixinxia@lnu.edu.cn*

[b]*Department of Chemical and Environmental Engineering, Yingkou Institute of Technology, Yingkou, 115014, Liaoning, China*

† Electronic supplementary information (ESI) available. See DOI: 10.1039/d1ra00974e

Experimental section

Fabrication of the $BiVO_4$ photoanode

A $BiVO_4$ electrode was prepared according to the electrodeposition method reported in literature.[24] 150 mL of deionized water was taken in a small beaker, and nitric acid was added to adjust the pH to 1.7. Then, 2.91 g of bismuth nitrate and 9.96 g of potassium iodide were added to the above mixture, and sonicated for about 30 min to fully dissolve. The above solution was mixed with an ethanol solution containing 0.23 M of *p*-benzoquinone, and sufficiently stirred to prepare an electrodeposition solution. An appropriate amount of the above-mentioned deposition solution was placed in a small beaker, and a three-electrode cell was used for electrodeposition (FTO was used as a working electrode, Pt was used as a counter electrode, and Ag/AgCl was used a reference electrode). At room temperature, after depositing for about 300 s at an applied bias of −0.1 V *vs.* Ag/AgCl, we obtained a BiOI film, which was washed with deionized water and blown with nitrogen. Then, a DMSO solution-containing 0.2 M acetylacetonoxane was added dropwise to the deposited layer, and calcined at 450 °C for 2 h (2 °C min^{-1}) to convert BiOI into $BiVO_4$. Finally, it was immersed in a 1 M aqueous solution of sodium hydroxide for about 10 min in order to remove excess V_2O_5, rinsed with deionized water, and blown dry with nitrogen for use.

Fabrication of the TaON/$BiVO_4$ photoanode

TaON nanoparticles were prepared by heating Ta_2O_5 particles at 1123 K for 15 h under NH_3 flow (20 mL min^{-1}).[25] A certain amount of TaON (1, 0.02 g; 2, 0.04 g; 3, 0.06 g) was added to 100 mL of deionized water, sonicated to make a sol, and the $BiVO_4$ photoanodes were separately immersed in different concentrations TaON sol at 60 °C for 1 h, and calcined at 500 °C for 2 h under N_2 flow.

Fabrication of the Co-Pi/TaON/$BiVO_4$ photoanode

The Co-Pi cocatalyst was loaded by photoelectron deposition according to literature.[26] The 2-TaON/$BiVO_4$ photoanode was immersed in a phosphate buffer solution-containing a certain concentration of $Co(NO_3)_2 \cdot 6H_2O$. Deposition was carried out at an applied bias of 0.1 V *vs.* Ag/AgCl and the sun illumination (100 mA cm^{-2}) for 300 s.

Characterization of photoanodes

The XRD pattern was measured used a Bruker D8 QUEST. The SEM images were recorded on a SU8000 Schottky field emission scanning electron microscope (SFE-SEM) equipped with a Rontec EDX system. The UV-Vis absorbance spectra were recorded on a Lambda 35 UV-Vis spectrophotometer. X-ray photoelectron spectra (XPS) were recorded on a Thermo Scientific ESCALAB 250 instrument (150 W, spot size of 500 μm and Al Kα radiation at 1486.6 eV) to obtain the surface elements. Photoluminescence (PL) spectroscopy measurement was performed on a Cary Eclipse spectrophotometer.

Photoelectrochemical measurements

The PEC performance tests of the electrodes were carried out using a standard three-electrode cell using an Ag/AgCl (3.5 M KCl) as the reference electrode, a platinum wire as the counter electrode and samples as the working electrode. The electrolyte used was a 0.1 M potassium buffer solution (pH 7.0) that was a mixture of mono- and dibasic hydrophosphates KH_2PO_4 and K_2HPO_4. The light intensity of the solar simulator (AM 1.5 G) was calibrated to 100 mW cm^{-2}. The effective surface area of the electrodes was 1 cm^2. The electrochemical impedance spectroscopy (EIS) was measured with the range from 0.1 Hz to 100 000 Hz. The Mott–Schottky curves were obtained under dark conditions, and the potential range was from −0.6 V to +1.0 V *vs.* Ag/AgCl.

The incident photon-to-current efficiency (IPCE) at each wavelength was determined at 1.23 V *vs.* RHE using monochromatic light illumination from a 300 W Xe arc lamp and neutral density filters simulating sunlight. The IPCE values have been calculated as follows:

$$\mathrm{IPCE} = \frac{J \times \lambda}{P_{\mathrm{light}}} \times 100\%$$

where J is the photocurrent density, λ is the incident light wavelength and P is the measured irradiance.

The applied bias photon-to-current efficiency (ABPE) was calculated from a *J–V* curve using the following equation:

$$\mathrm{ABPE} = \frac{J \times (1.23 - V_{\mathrm{bias}})}{P_{\mathrm{in}}} \times 100\%$$

where J is the photocurrent density, V_{bias} is the applied bias and P_{in} is the incident illumination power density (AM 1.5 G, 100 mW cm^{-2}).

The total water oxidation photocurrent J_{H_2O} was determined by the following expression:

$$J_{H_2O} = J_{\mathrm{abs}} \times \eta_{\mathrm{sep}} \times \eta_{\mathrm{trans}}$$

where J_{abs} is the photocurrent density when the absorbed photons completely converted into current, η_{sep} is the charge separation efficiency, and η_{trans} is the surface charge transfer efficiency.

To obtain η_{trans}, Na_2SO_3 was added into the 0.1 M PBS electrolyte, which was an efficient hole scavenger. Therefore, the η_{trans} efficiency equal to 1, and the photocurrent could be described as $J_{Na_2SO_3} = J_{\mathrm{abs}} \times \eta_{\mathrm{sep}}$. So, the η_{sep} could be described as:

$$\eta_{\mathrm{sep}} = J_{Na_2SO_3}/J_{\mathrm{abs}}.$$

The η_{trans} was calculated using the equation:

$$\eta_{\mathrm{trans}} = J_{H_2O}/J_{Na_2SO_3}$$

where J_{H_2O} is the photocurrent density of the TaON/$BiVO_4$ electrode in 0.1 M PBS, and $J_{Na_2SO_3}$ is the photocurrent density of the TaON/$BiVO_4$ electrode in 0.1 M PBS containing 0.1 M Na_2SO_3.

Results and discussion

$BiVO_4$ films were fabricated *via* the electrochemical-deposition method. TaON nanoparticles were loaded onto the $BiVO_4$ surface, as shown in Scheme 1. By controlling the amount of TaON nanoparticles, different TaON/$BiVO_4$ electrodes were fabricated (denoted as 1-TaON/$BiVO_4$, 2-TaON/$BiVO_4$ and 3-TaON/$BiVO_4$, respectively). The microstructure of the pristine $BiVO_4$ is shown in Fig. 1a. A porous structure could be seen clearly in the whole area, which guaranteed the combination with TaON nanoparticles. The SEM images of TaON/$BiVO_4$ electrodes containing different amounts of TaON are shown in Fig. 1. The distribution density of TaON nanoparticles increased with the amount of TaON (Fig. 1b–d). The crystal structures of the TaON, $BiVO_4$ and TaON/$BiVO_4$ samples were tested by X-ray diffraction (XRD) patterns, as shown in Fig. S1,† confirming that TaON has been successfully modified on the $BiVO_4$ electrode.

X-ray photoelectron spectroscopy (XPS) was performed to investigate the chemical states of the TaON/$BiVO_4$ electrodes. Ta, O, N, Bi and V elements were detected and shown in Fig. 2. Compared to the pristine $BiVO_4$, the characteristic signals of TaON can be observed in the spectrum of the TaON/$BiVO_4$ electrode. The characteristic peaks of N 1s and Ta 4p are shown in Fig. 2a. The binding energies of 529.7 eV and 532.0 eV are assigned to the O 1s of $BiVO_4$, and the O 1s peak of TaON appears at 530.6 eV (Fig. 2b). The binding energies of 159.1 eV and 164.4 eV were assigned to the $4f_{7/2}$ and $4f_{5/2}$ of the Bi element, confirming that the Bi element was present as Bi^{3+} (Fig. 2c).[27] The binding energies for the V $2p_{3/2}$ and V $2p_{1/2}$ located at 516.6 and 524.2 eV were typical values for V^{5+} (Fig. 2d).[28] The Bi 4f and V 2p peaks of the TaON/$BiVO_4$ electrode shifted positively compared to that of the $BiVO_4$ electrode, indicating an interaction between TaON and $BiVO_4$.

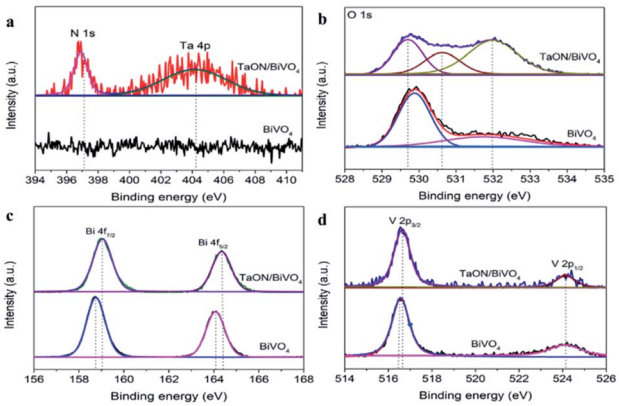

Fig. 2 XPS spectra of $BiVO_4$ and TaON/$BiVO_4$ electrodes: (a) N 1s, Ta 4p, (b) O 1s, (c) Bi 4f, (d) V 2p.

The PEC measurements of $BiVO_4$ and TaON/$BiVO_4$ were carried out using a three-electrode system under simulated solar light 100 mW cm^{-2}. The linear sweep voltammetry (LSV) curves of the sample electrodes are shown in Fig. 3a. The photocurrent density of TaON/$BiVO_4$ electrodes was significantly higher than that of the bare $BiVO_4$ electrode. The 2-TaON/$BiVO_4$ photoanode showed the highest photocurrent density, reaching 2.6 mA cm^{-2} at 1.23 V *vs.* RHE, which was 1.75-times that of bare $BiVO_4$. However, the photocurrent density of 3-TaON/$BiVO_4$ was lower than that of 2-TaON/$BiVO_4$, suggesting that excessive TaON nanospheres hindered the charge transfer. The applied bias photon-to-current efficiencies (ABPEs) of $BiVO_4$ and TaON/$BiVO_4$ electrodes were calculated by the LSV curves (Fig. 3b). The maximum value of the 2-TaON/$BiVO_4$ electrode reached 0.61% at 0.74 V, about 3-times of the $BiVO_4$ electrode (0.19% at 0.95 V).

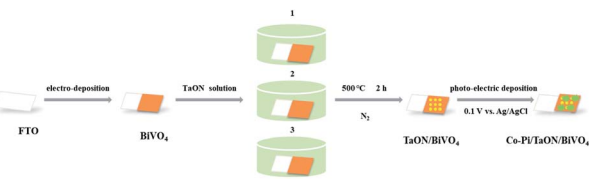

Scheme 1 An illustration of the preparation of TaON/$BiVO_4$ and Co-Pi/2-TaON/$BiVO_4$ electrodes.

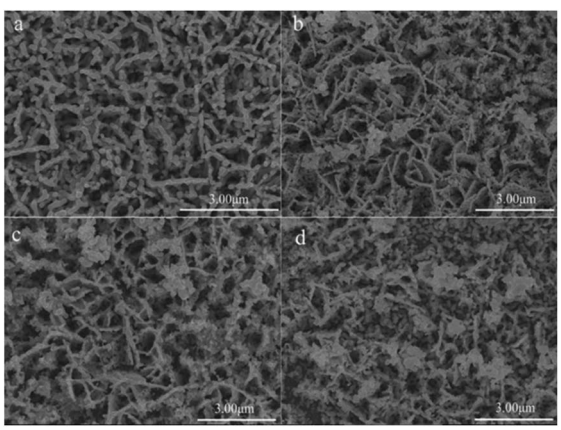

Fig. 1 SEM images of different electrodes. (a) $BiVO_4$, (b) 1-TaON/$BiVO_4$, (c) 2-TaON/$BiVO_4$, (d) 3-TaON/$BiVO_4$.

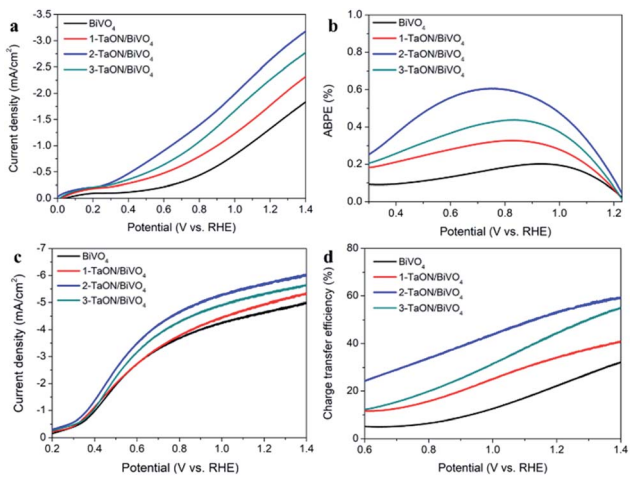

Fig. 3 (a) LSV curves in the PBS solution, (b) ABPE values, (c) LSV curves in the PBS solution containing 0.1 M Na_2SO_3 and (d) the charge transfer efficiencies of different electrodes.

In order to measure the charge recombination of the TaON/$BiVO_4$ electrodes, 0.1 M Na_2SO_3 was added into the electrolyte as a hole scavenger for the PEC measurement.[29] The introduction of Na_2SO_3 can eliminate the surface charge recombination. The PEC measurement results are shown in Fig. 3c. Compared to the bare $BiVO_4$ electrode, all the TaON/$BiVO_4$ electrodes showed higher photocurrent, which indicated that the combination of the two semiconductors produced a better charge separation. The 2-TaON/$BiVO_4$ electrode showed the highest photocurrent density of 5.6 mA cm^{-2} at 1.23 V *vs.* RHE. Based on the LSV curves, the separation and surface charge transfer efficiencies of the sample electrodes are calculated and shown in Fig. S4† and 3d, respectively. All the TaON/$BiVO_4$ electrodes exhibited higher η_{sep} and η_{trans} than the bare $BiVO_4$. 2-TaON/$BiVO_4$ showed the highest values. These results indicated that the construction of TaON/$BiVO_4$ could promote both charge separation and surface charge transfer.

The incident photon-to-current conversion efficiency (IPCE) values are shown in Fig. S2.† In the visible spectrum, TaON/$BiVO_4$ showed a higher IPCE value than $BiVO_4$. At 520 nm, the IPCE value dropped to 0, which was consistent with the absorption spectra (Fig. S3†).

In order to understand the charge transfer characteristics of TaON/$BiVO_4$ and $BiVO_4$ electrodes, electrochemical impedance spectroscopy (EIS) tests were performed in 0.1 M PBS at 1.23 V. Smaller semicircles represent better charge transfer capabilities and faster surface reaction kinetics. As shown in Fig. 4a, the $BiVO_4$ electrode exhibited the largest semicircle among all electrodes, indicating the highest interface charge transfer barrier. Three sample TaON/$BiVO_4$ electrodes showed smaller charge transfer resistance than the $BiVO_4$ electrode, further confirming that TaON was beneficial to improve the charge transfer. The interface charge transfer resistance (R_{ct}) of the sample electrodes is shown in Table S1.† 2-TaON/$BiVO_4$ showed the smallest charge transfer resistance, which was in accordance with the photocurrents.

To investigate the charge transfer behavior between $BiVO_4$ and TaON, photoluminescence (PL) measurements were performed. As shown in Fig. 4b. $BiVO_4$ electrode exhibited a high-intensity characteristic emission, suggesting an obvious radiative charge recombination. However, the TaON/$BiVO_4$ electrode exhibited much lower emission intensity. The obvious photoluminescence quenching for TaON/$BiVO_4$ electrode fully proved the formation of TaON/$BiVO_4$ heterojunctions.

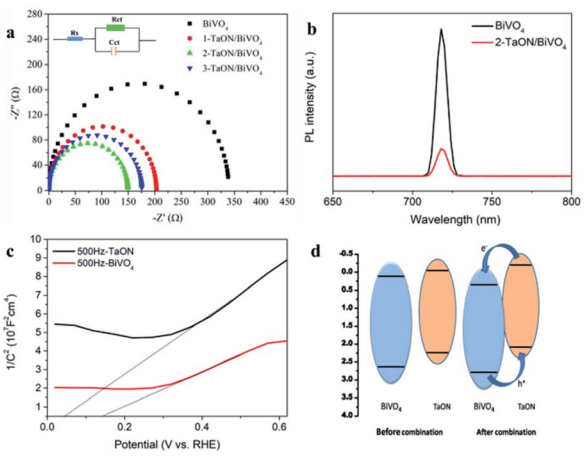

Fig. 4 (a) Electrochemical impedance spectroscopy (EIS) of different electrodes. (b) PL measurements of the $BiVO_4$ and 2-TaON/$BiVO_4$ electrode (exciting source: 360 nm). (c) The Mott–Schottky plots of $BiVO_4$ and TaON. (d) The charge transfer mechanism of the TaON/$BiVO_4$ electrode.

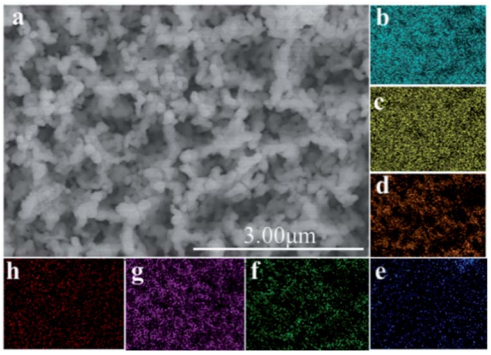

Fig. 5 SEM image of the Co-Pi/TaON/$BiVO_4$ electrode (a) and the EDS-mapping element of the Co-Pi/TaON/$BiVO_4$ electrode. (b) Bi, (c) V, (d) O, (e) Ta, (f) N, (g) Co, (h) P.

The Mott–Schottky plots of $BiVO_4$ and TaON were also measured. As shown in Fig. 4c, it can be seen that the CB positions of $BiVO_4$ and TaON are 0.15 eV and 0.05 eV. The band gap width of $BiVO_4$ and TaON obtained from the absorption spectrum were 2.41 eV and 2.16 eV, respectively (Fig. S5†). The valence band positions of $BiVO_4$ and TaON can be calculated by the formula using $E_{CB} = E_{VB} - E_g$, which were 2.56 eV and 2.21 eV. The CB edge potential of TaON was more negative than that of $BiVO_4$. Thus, a difference of band potentials existed between the two materials, and a contact electric field was built at the interface of the TaON and $BiVO_4$. When electrons and holes were photogenerated, as shown in Fig. 4d, driven by the contact electric field, electrons transferred from TaON to $BiVO_4$ and holes transferred from $BiVO_4$ to TaON, thereby leading to an enhancement both in photogenerated charge separation and transfer.

In order to further enhance the PEC performance, Co-Pi, which is well-used as highly efficient catalyst in PEC water oxidation, was equipped onto the TaON/$BiVO_4$ electrode. The SEM image of the Co-Pi/TaON/$BiVO_4$ electrode showed that Co-Pi appeared to be discontinuous particles (Fig. 5a). The EDS-mapping (Fig. 5b–h) suggested the existence of Bi, V, O, Ta, N, Co, and P elements, indicating the successful fabrication of the Co-Pi/TaON/$BiVO_4$ electrode. According to the LSV curves shown in Fig. 6a, an obviously increased photocurrent density was obtained for the Co-Pi/TaON/$BiVO_4$ photoanode, achieving 3.6 mA cm^{-2} at 1.23 V *vs.* RHE, which was about 3-times higher than that of the $BiVO_4$ electrode. During a potentiostatic electrolysis at 0.8 V *vs.* RHE, the bare $BiVO_4$ electrode always exhibited very low photocurrent density. For Co-Pi/TaON/$BiVO_4$ high activity and stability was observed for more than 6000 s (Fig. S6†). The half-cell photoconversion efficiency of the Co-Pi/TaON/$BiVO_4$ electrode achieved 1.19% at 0.69 V (Fig. 6a), approximately 6-times compared to that of $BiVO_4$ electrode.

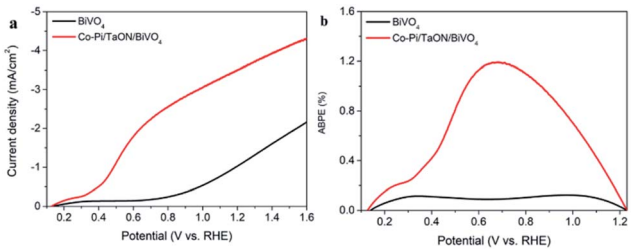

Fig. 6 LSV curves (a) and ABPE values (b) of $BiVO_4$ and Co Pi/TaON/$BiVO_4$ electrodes.

Conclusions

In summary, we have successfully fabricated TaON/$BiVO_4$ heterojunction electrodes by integrating TaON nanoparticles onto $BiVO_4$ electrodes. The as-prepared TaON/$BiVO_4$ electrodes exhibited significantly higher performances for PEC water oxidation. The 2-TaON/$BiVO_4$ electrode showed the highest photocurrent, reaching 2.6 mA cm^{-2} at 1.23 V *vs.* RHE, 1.75 times that of the bare $BiVO_4$ electrode. In order to further increase the photocurrent, a Co-Pi water oxidation catalyst was attached onto the TaON/$BiVO_4$ electrode. A high photocurrent density as high as 3.6 mA cm^{-2} (1.23 V *vs.* RHE) was obtained, and the half-cell photoconversion efficiency achieved 1.19% at 0.69 V, approximately 6-times that of the $BiVO_4$ photoanode. This study provides a promising route to achieve highly efficient PEC water splitting in designing solar-to-fuel conversion devices.

Conflicts of interest

There are no conflicts to declare.

Acknowledgements

This work was supported by the National Natural Science Foundation of China (21671089), the Liaoning Revitalization Talents Program (XLYC1807210), the Natural Science Foundation of Liaoning Province of China (2020-YKLH-22) and the Scientific Research Fund of Liaoning Provincial Education Department (L2020002).

Notes and references

1 M. E. El-Khouly, E. El-Mohsnawy and S. Fukuzumi, *J. Photochem. Photobiol., C*, 2017, **31**, 36–83.
2 P. D. Frischmann, K. Mahata and F. Wurthner, *Chem. Soc. Rev.*, 2013, **42**, 1847–1870.
3 J. Qi, W. Zhang and R. Cao, *Adv. Energy Mater.*, 2018, **8**, 1701620.
4 R. L. Charles and M. B. Bart, *Acc. Chem. Res.*, 2016, **49**, 1121–1129.
5 Y. Yi, N. Shuwen, H. Dongdong, L. Tianyu, W. Gongming and L. Yat, *Adv. Energy Mater.*, 2017, **7**, 1700555.
6 W. Wei, X. Meigui, X. Xiaomin, Z. Wei and S. Zongping, *Angew. Chem., Int. Ed.*, 2019, **5**, 136–152.
7 M. Nurul Aida, S. Javad, I. Aznan Fazli, K. Muhammad Najib, J. Muhammad Fareez Amir Mohd, N. Mohamad Firdaus Mohamad, A. Nurul Affiqah, Z. Di, S. S. Jagdeep and T. Mohd Asri Mat, *Mater. Res. Bull.*, 2020, **125**, 110779.
8 Z. Bo, Z. Haipeng, W. Zeyan, Z. Xiaoyang, Q. Xiaoyan, D. Ying, L. Yuanyuan, W. Peng, L. Yingjie and H. Baibiao, *Appl. Catal., B*, 2017, **211**, 258–265.
9 G. Qiqian, S. Xiaojuan, Y. Xijia, W. Liying, L. Xuesong, Z. Xueyu, D. Lianfeng and L. Wei, *New J. Chem.*, 2019, **43**, 8551–8556.
10 S. Bo, S. Tielin, L. Zhiyong, T. Zirong, Z. Jianxin and L. Guanglan, *RSC Adv.*, 2016, **6**, 110120–110126.
11 D. Paula, L. Tânia, M. Laura, A. Luísa and M. Adélio, *Phys. Chem. Chem. Phys.*, 2016, **18**, 5232–5243.
12 K. C. Jason, G. Sheraz, M. T. Francesca, C. Le, L. Yi-Sheng, G. Jinghua, W. A. Joel, Y. Junko and D. S. Ian, *J. Phys. Chem. C*, 2015, **119**, 2969–2974.
13 P. Yuriy, T. Ivan, M. Kazuma, U. Jin, K. Yutaka, K. Sonya, M. Kikuo, S. Takeyoshi, M. Takuya, F. Daisuke, T. Masahiro, K. Michio and K. Takehiko, *Sci. Rep.*, 2015, **8**, 11141.
14 A. P. Blaise, D. B. Jesse, C. S. Linsey, J. F. Arnold, C. Zhebo, G. D. Todd, D. J. Brian, N. B. Kevin, N. B. George, A. Shane, W. Heli, M. Eric and F. J. Thomas, *Energy Environ. Sci.*, 2013, **6**, 1983–2002.
15 H. Baobing, L. Yuchuan, H. Xing and X. Zailai, *J. Mater. Chem. A*, 2018, **6**, 22277–22286.
16 S. Xia, Z. Yu and J. Jiang, *Chem. Commun.*, 2019, **55**, 4813–4816.
17 K. Eun Sun, K. Hyun Joon, M. Ganesan, K. Jae Young, J. Ji-Wook and L. Jae Sung, *ACS Appl. Mater. Interfaces*, 2014, **6**, 17762–17769.
18 J. Su, X.-X. Zou, G.-D. Li, X. Wei, C. Yan, Y.-N. Wang, J. Zhao, L.-J. Zhou and J.-S. Chen, *J. Phys. Chem. C*, 2011, **115**, 8064–8071.
19 K. Ding, B. Chen, Z. Fang, Y. Zhang and Z. Chen, *Phys. Chem. Chem. Phys.*, 2014, **16**, 13465–13476.
20 Y. Pihosh, I. Turkevych, K. Mawatari, T. Asai, T. Hisatomi, J. Uemura, M. Tosa, K. Shimamura, J. Kubota, K. Domen and T. Kitamori, *Small*, 2014, **10**, 3692–3699.
21 S. J. Hong, S. Lee, J. S. Jang and J. S. Lee, *Energy Environ. Sci.*, 2011, **4**, 1781–1787.
22 Y. B. Cheng, S. J. Yang, W. H. Cho and J. J. Wu, *ACS Appl. Mater. Interfaces*, 2016, **8**, 20032–20039.
23 M. Xie, X. Fu, L. Jing, P. Luan, Y. Feng and H. Fu, *Adv. Energy Mater.*, 2014, **4**, 1300995.
24 K. Tae Woo and C. Kyoung-Shin, *Science*, 2014, **343**, 990–994.
25 M. Higashi, K. Domen and R. Abe, *Energy Environ. Sci.*, 2011, **4**, 4138–4147.
26 K. Z. Diane, C. Maurin, S. Kevin, G. Michael and R. G. Daniel, *Energy Environ. Sci.*, 2011, **16**, 1759–1764.
27 D. Long, G. Shuai, Z. Suiyi, X. Dongfang, Z. Leilei, H. Mingxin and Y. Xia, *Catal. Commun.*, 2011, **16**, 250–254.
28 G. Yingna, Y. Xia, M. Fengyan, L. Kexin, X. Lei, Y. Xing and G. Yihang, *Appl. Surf. Sci.*, 2009, **256**, 2215–2222.
29 K. D. Zhong, S. Choi and R. D. Gamelin, *J. Am. Chem. Soc.*, 2011, **133**, 18370–18377.